DNS study of scalar transport in a compressible turbulent jet

Pratik Nayak

p.v.nayak@tudelft.nl

Talk at Earth and Planetary Magnetism group, ETH Zürich

19th June, 2017

Overview

Turbulent Jet ?

- Class of free turbulent flows.
- Applications include jet exhausts, industrial mixing processes, combustion etc,.
- Reynolds number can range from 1000 to 10^6 and higher.
- Scalar transport usually present, both active and passive.

How does it look? [Credit: The Slow Mo guys (youtube)]

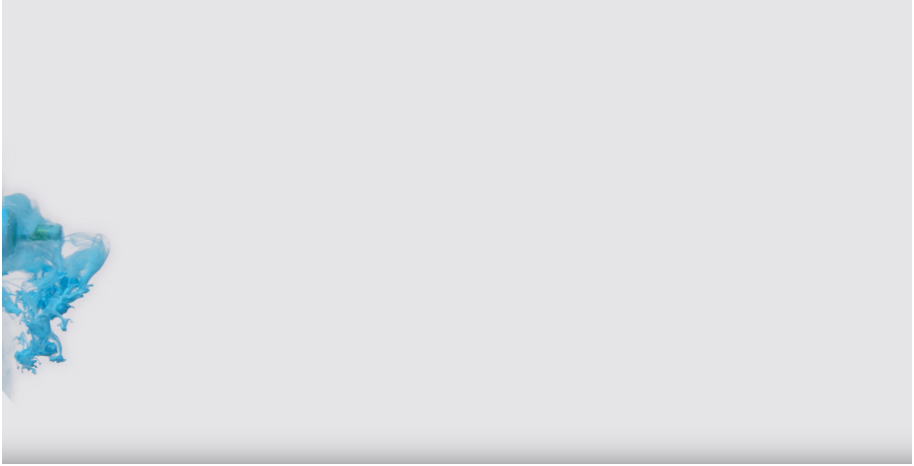

Objectives

1. Identify issues faced with scalar transport modeling for turbulent jets at high Reynolds numbers.
2. Develop and implement a method to accurately model the scalar transport phenomena.
3. Compare the improvement in the model with the previous methods and report on the results.

Our setting

- A compressible high Re, high Ma number flow.
- Direct Numerical Simulation.
- Navier–Stokes–Fourier system with additional Scalar transport equation.
- A full 3D flow.

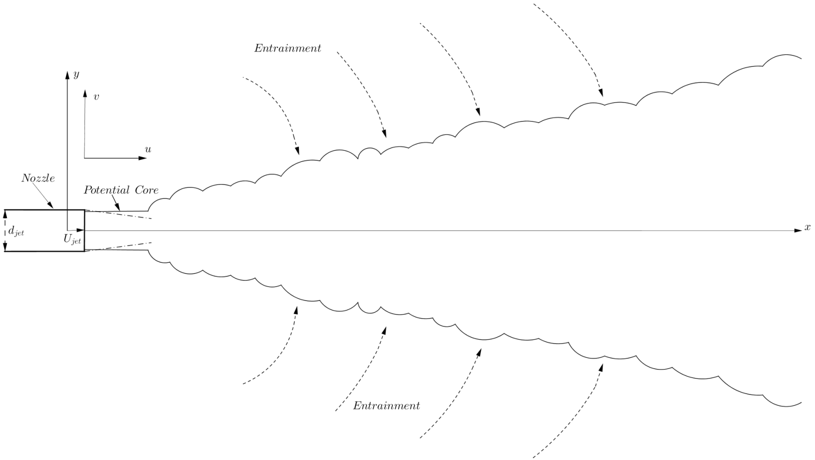

Figure: The free turbulent jet schematic

Navier–Stokes–Fourier system

Mass:

$$\frac{\partial \rho}{\partial t} + \frac{\partial}{\partial x_j}(\rho u_j) = 0 \tag{1}$$

Momentum:

$$\frac{\partial \rho u_i}{\partial t} + \frac{\partial}{\partial x_j}(\rho u_i u_j + p\delta_{ij}) = \frac{\partial \tau_{ij}}{\partial x_j} \tag{2}$$

Energy:

$$\frac{\partial E}{\partial t} + \frac{\partial}{\partial x_j} u_j(p + E) = \frac{\partial}{\partial x_j}\kappa\frac{\partial T}{\partial x_j} + \frac{\partial u_i \tau_{ij}}{\partial x_j} \tag{3}$$

Scalar transport:

$$\frac{\partial \rho Y_k}{\partial t} + \frac{\partial \rho u_j Y_k}{\partial x_j} = \frac{\partial}{\partial x_j}\left(\rho\kappa_{scal}\frac{\partial Y_k}{\partial x_j}\right) + \omega_k \tag{4}$$

Reynolds number effects

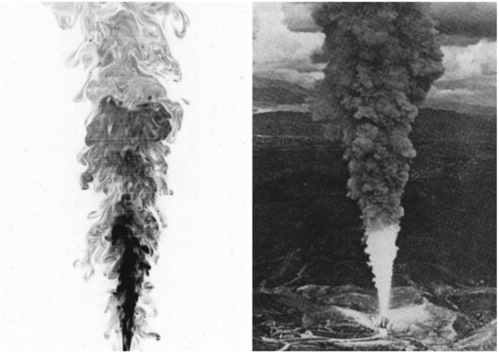

Figure: The effect of Reynolds number, Left: $\mathrm{Re} = 2 \times 10^3$, Right: $\mathrm{Re} = 2 \times 10^8$

$$\frac{\mathcal{L}}{\eta} \sim Re^{3/4} \tag{5}$$

Spatial discretization - compact finite difference

Derivative:

$$\alpha f'_{i-1} + f'_i + \alpha f'_{i+1} = d\frac{f_{i+7/2} - f_{i-7/2}}{h} + c\frac{f_{i+5/2} - f_{i-5/2}}{h} + b\frac{f_{i+3/2} - f_{i-3/2}}{h} + a\frac{f_{i+1/2} - f_{i-1/2}}{h} \tag{6}$$

Interpolation:

$$\alpha f_{i-1} + f_i + \alpha f_{i+1} = d(f_{i+7/2} + f_{i-7/2}) + c(f_{i+5/2} + f_{i-5/2}) + b(f_{i+3/2} + f_{i-3/2}) + a(f_{i+1/2} + f_{i-1/2}) \tag{7}$$

1. Tri-diagonal linear systems.
2. Spectral-like resolution, suitable for turbulent flows [Lele, 1992].
3. Staggered grid [Boersma, 2005].

Grids - Staggered and Co-located

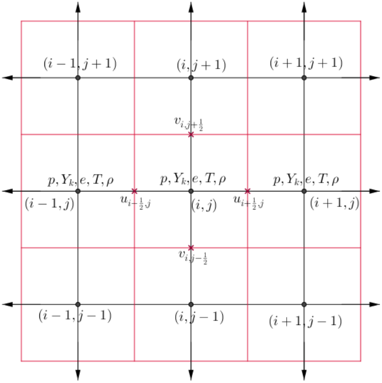

(a) Staggered discretization grid

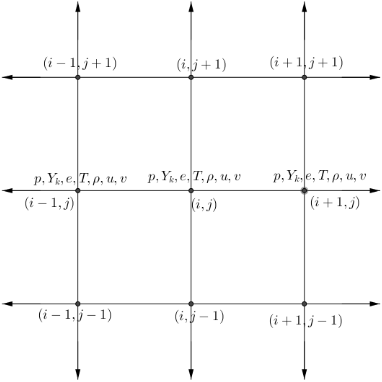

(b) Co-located discretization grid

Figure: 2D grid for discretization

Why are Non-oscillatory methods required ?

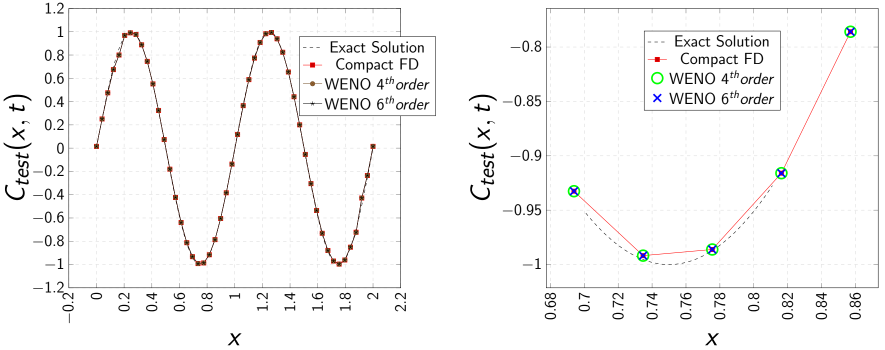

(a) Sine wave (b) Sine wave: Focussed

Figure: Numerical Tests: Comparison of WENO with central compact schemes, 1

Why are Non-oscillatory methods required ?

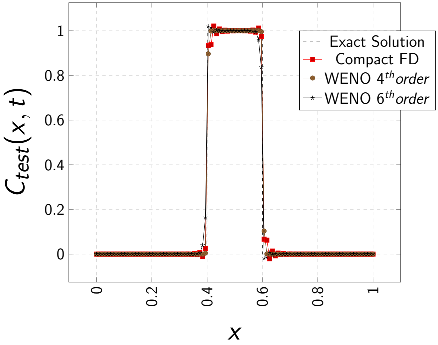

(a) Square wave

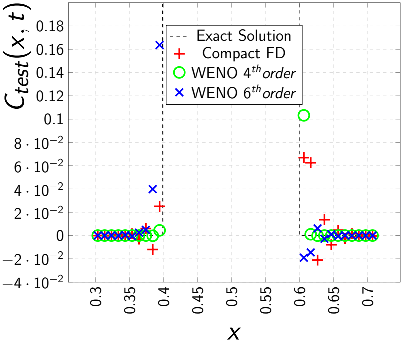

(b) Square wave: Focussed

Figure: Numerical Tests: Comparison of WENO with central compact schemes, 2

ENO and WENO

Stencils:

$$S_r(i) = \{x_{i-r}, ..., x_{i-r+k-1}\}, \qquad r = 0, ..., k-1 \tag{8}$$

Non-linear weighting:

$$v_{i+\frac{1}{2}} = \sum_{j=0}^{k-1} \omega_r v_{i+\frac{1}{2}}^{(r)} \tag{9}$$

$$\omega_r \geq 0; \qquad \sum_{r=0}^{k-1} \omega_r = 1 \tag{10}$$

$$\omega_r = \frac{\alpha_r}{\sum_{s=0}^{k-1} \alpha_s}, \qquad r = 0, ..., k-1 \tag{11}$$

$$\alpha_r = \frac{d_r}{(\epsilon + \beta_r)^2}, \qquad \beta_r = \sum_{l=1}^{k-1} \int_{x_{i-\frac{1}{2}}}^{x_{i+\frac{1}{2}}} \Delta x^{2l-1} \left(\frac{\partial^l p_r(x)}{\partial^l x} \right)^2 dx \tag{12}$$

Hybrid-compact WENO

Linear Hybrid:

$$\tilde{f}^{hyb}_{i+\frac{1}{2}} = (1-\sigma)\tilde{f}^{upw}_{i+\frac{1}{2}} + \sigma \tilde{f}^{cent}_{i+\frac{1}{2}} = \sum_{j=0}^{k} y_j \tilde{f}^{j}_{i+\frac{1}{2}} \tag{13}$$

$$\sigma = min\left(1, \frac{\varrho_{i+\frac{1}{2}}}{\varrho_c}\right) \tag{14}$$

$$\varrho_{i+\frac{1}{2}} = min(\varrho_{i-1}, \varrho_i, \varrho_{i+1}, \varrho_{i+2}) \tag{15}$$

$$\varrho_i = \frac{|2(f_{i+1}-f_i)(f_i-f_{i-1})| + \delta}{(f_{i+1}-f_i)^2 + (f_i - f_{i-1})^2 + \delta} \tag{16}$$

Hybrid WENO:

$$\tilde{f}^{hyb}_{i+\frac{1}{2}} = \sum_{j=0}^{k} \omega_j \tilde{f}^{j}_{i+\frac{1}{2}} \tag{17}$$

Flux splitting

1. Upwinding requires information from the correct domain of dependence.

Flux is

$$f(u) = f^{+}(u) + f^{-}(u) \tag{18}$$

where

$$\frac{df^{+}(u)}{du} \geq 0 \qquad \frac{df^{-}(u)}{du} \leq 0 \tag{19}$$

Lax-Friedrichs:

$$f^{\pm}(u) = \frac{1}{2}(f(u) \pm \alpha u \quad ; \quad \alpha = \max(|f'(u)|) \tag{20}$$

Flux splitting

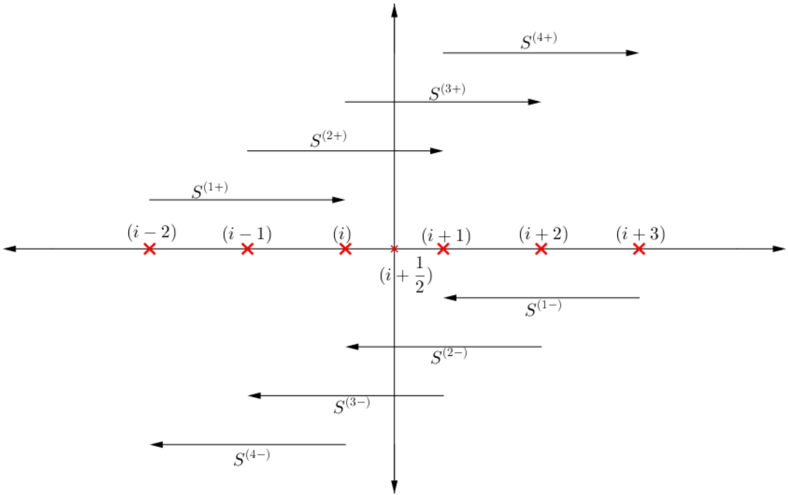

Figure: Stencils for flux splitting

Temporal discretization

Runge–Kutta, explicit method

$$U^{n+1} = U^n + \Delta t \sum_{i=0}^{s} b_i K_i \tag{21}$$

Table: Butcher Tableau - RK4

$$\begin{array}{c|cccc} 0 & & & & \\ \frac{1}{2} & \frac{1}{2} & & & \\ \frac{1}{2} & 0 & \frac{1}{2} & & \\ 1 & 0 & 0 & 1 & \\ \hline & \frac{1}{6} & \frac{1}{3} & \frac{1}{3} & \frac{1}{6} \end{array}$$

Boundary conditions

1. Inflow and outflow: addition of locally supersonic axial velocity.
2. Lateral boundaries: Damping required to eliminate reflections from boundaries.

$$-A(x, y, z)(\mathfrak{Q} - \mathfrak{Q}_{tar}) \tag{22}$$

3. Additional filtering to remove high wavenumber components using a compact filter.
4. Lagrange extrapolation at boundaries to calculate ghost points for WENO interpolation.

Boundary conditions: Inflow and outflow

1. Inflow :

$$
\begin{aligned}
u &= \frac{Ma}{2}\left(1 - \tanh\left[B\left(\frac{r}{r_{jet}} - \frac{r_{jet}}{r}\right)\right]\right);\ v = 0;\ w = 0 \\
\rho &= 1 + \left(\frac{T_0}{T_{jet}}\right)\frac{u}{Ma} \\
E &= \frac{1}{\gamma(\gamma-1)} + \frac{1}{2}\rho u^2 \\
Y_k &= \begin{cases} 1.0 & , d \leq d_{jet} \\ 0.0 & , \text{else} \end{cases}
\end{aligned}
\tag{23}
$$

$$
B = B(\theta, t) = B_0 + \sum_m \sum_n \mathfrak{B}_{nm} \cos(f_{nm} t + \phi_{nm}) cos(m\theta + \psi_{nm}) \tag{24}
$$

Parallelized using MPI

1. Domain decomposed using the `2decomp` library.

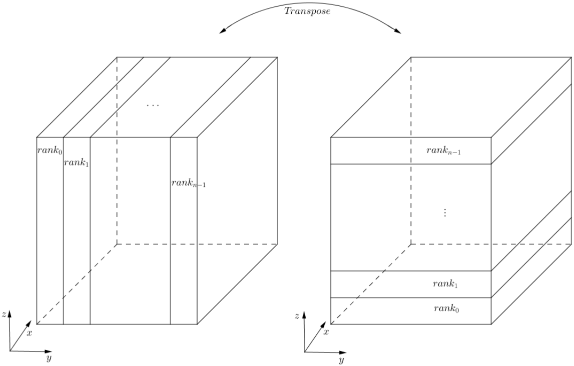

Figure: Domain Decomposition

Efficiency ?

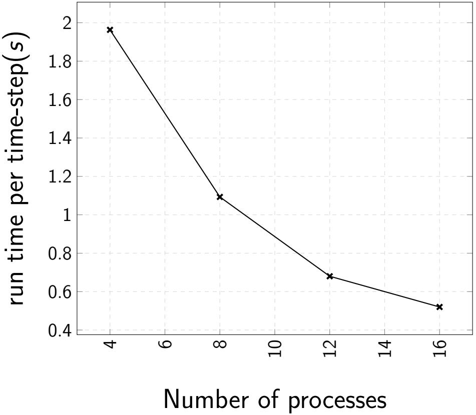

Figure: Strong scaling test, Problem size: $128 \times 64 \times 64$

Improvement in solution

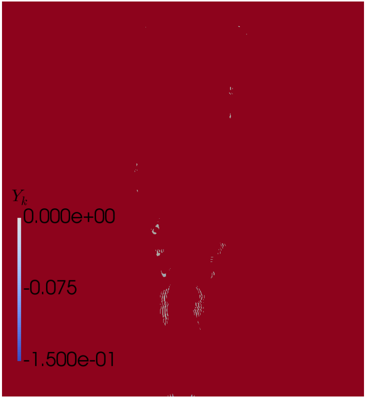

(a) Compact FD

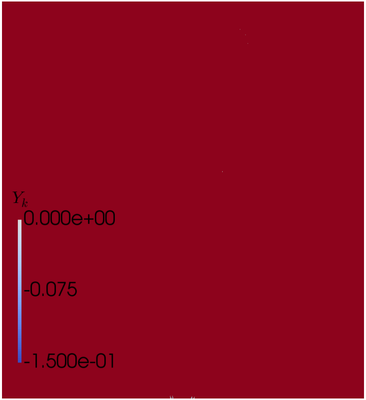

(b) Compact WENO

Figure: Oscillations in scalar concentration, Y_k fields, Re $= 8500$

Method comparisons

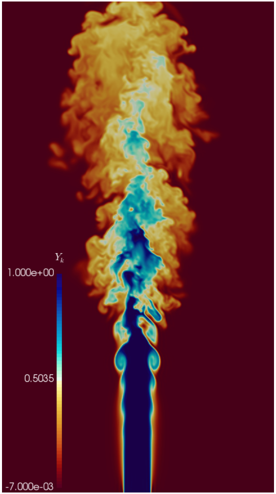

(a) Scalar concentration: Compact FD

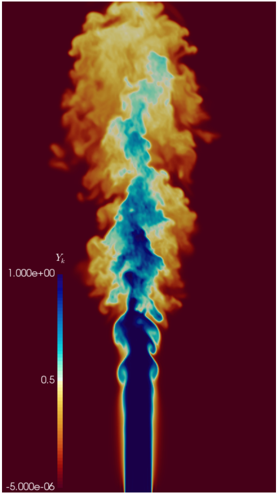

(b) Scalar concentration: WENO, low dissipation

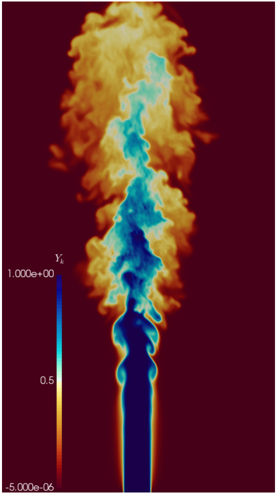

(c) Scalar concentration: WENO, high dissipation

Validation with experiments

Grid size: 960 x 480 x 480; $\Delta t = 1/200$; CFL ~ 0.5

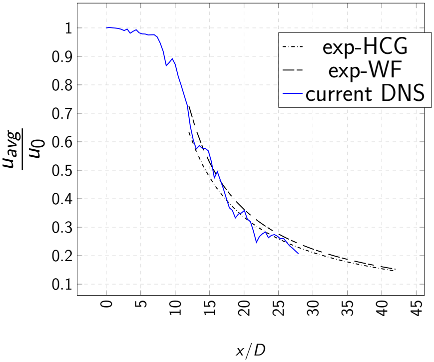

(a) 1/X behaviour

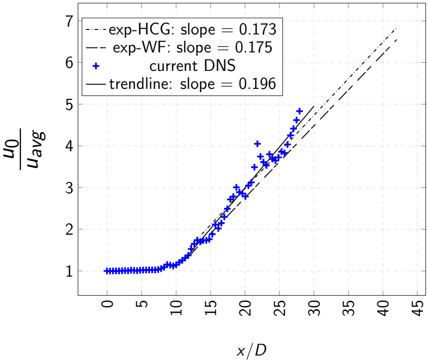

(b) Decay rates

Figure: Comparison with experimental results at Re $= 1 \times 10^4$, y normal

Decay rates

1. Expected decay rate: Between 5.0 and 5.9 for a compressible turbulent jet, [Bodony,2004].

Method	**Decay rate**
Experimental, HCG	5.78
Experimental, WF	5.71
Current DNS	5.11

Table: Decay rates of NACV at $Re = 1 \times 10^4$

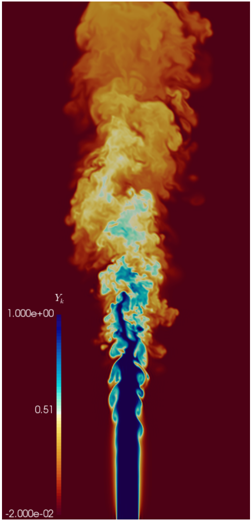

(a) Compact FD, Sc = 1.0

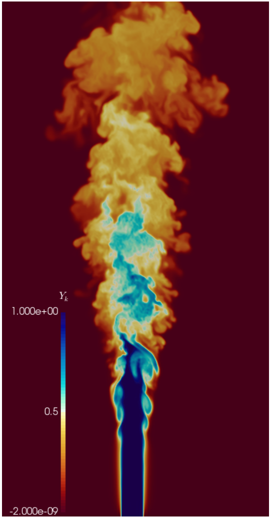

(b) Compact WENO, Sc = 1.0

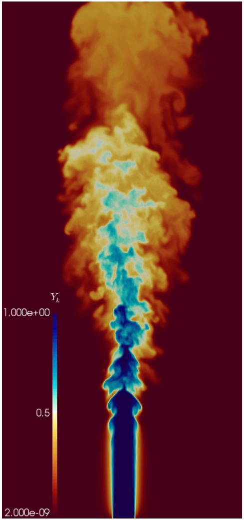

(c) Compact WENO, Sc = 0.5

Figure: Scalar concentration, Y_k fields, Re = 8500

Gaussian type behaviour of averaged axial velocities

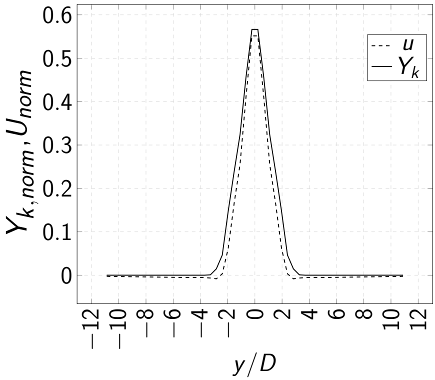

(a) WENO, Sc = 1.0, at $x/D = 12$

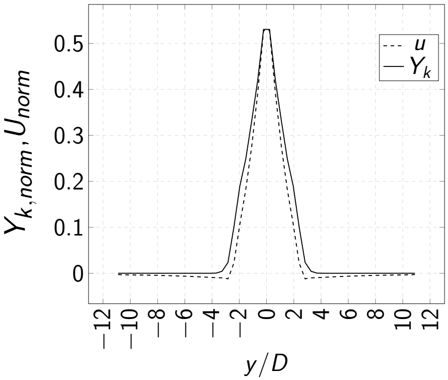

(b) WENO, Sc = 0.5, at $x/D = 12$

Figure: Comparison of WENO at Sc = 0.5 and Sc = 1.0 at Re = 8500

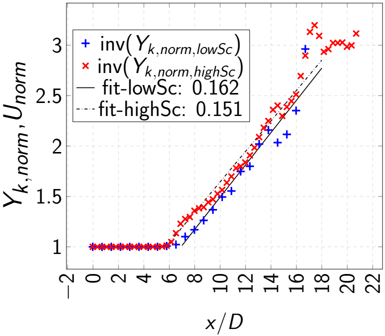

Figure: Decay rates for Sc= 1.0 and Sc = 0.5.

Method	**Decay rate**
Compact WENO, Sc = 1.0	6.62
Compact WENO, Sc = 0.5	6.17

Table: Decay rates of NACC at Re = 8.5×10^3

Conclusions

1. Central methods produce unphysical oscillations for problems of hyperbolic nature.
2. A WENO or ENO interpolation can remove these oscillations.
3. Using a hybrid WENO reduces dissipation and allows for a wider range of scales to be captured.
4. Decay rate of between 5 to 5.9 as expected for axial velocity.
5. A higher decay rate for the concentration close to 6 as previously observed. [Boersma, 1998]
6. Gaussian type profile for axial velocity perpendicular to flow axis.
7. Instability modes depend on Schmidt numbers, only one type can dominate the flow.
8. Lower Schmidt number: Varicose mode, Higher Schmidt number: Helical mode.

Thank You

Any questions ?

p.v.nayak@tudelft.nl